A Review of Anisotropic Polar Ice Models: from Crystal to Ice-Sheet Flow Models

Olivier Gagliardini, Fabien Gillet-Chaulet, Maurine Montagnat

LGGE CNRS / UJF-Grenoble I, BP 96, F-38402 Saint-Martin d'Hères Cedex, France, gagliar@glaciog.ujf-grenoble.fr

Abstract: The ice single crystal is one of the most anisotropic natural materials and the resulting viscous behaviour of polycrystalline ice can also be strongly anisotropic and is a function of the distribution of the crystal c-axis orientations, *i.e.* its fabric. Such a strong and strain-dependant anisotropy of the ice polycrystal certainly affects the general flow of polar ice. The aim of this paper is to present an exhaustive overview of most of the glaciological efforts made from more than two decades to account for polar ice anisotropy in ice flow modelling, from the crystal to the ice-sheets scale. We first recall the deformation and recrystallization processes occurring within ice-sheets and their respective effect on the polar ice textures. Then, the different models developed to describe the behaviour of the ice crystal and the polycrystal are presented, with a special emphasis on homogenization methods and fabric description. Finally, existing anisotropic ice flow models and their applications are reviewed.

Key words: Anisotropic model, Crystal, Fabric, Polycrystal, Ice

1 Introduction

The ice single crystal is one of the most anisotropic natural materials. This strong anisotropy results essentially from dislocation glide on the basal plane, perpendicular to the crystal hexagonal symmetry axis, called the c-axis. During the gravity driven flow of ice within an ice-sheet, the polycrystal develops a strain-induced fabric, that is, a preferred orientation of the c-axes of its grains. Near the surface, polycrystalline ice results from the transformation of deposited snow, and since the ice crystals are distributed at random, its mechanical behaviour is isotropic. Observations of deep ice cores drilled in Antarctica and Greenland have shown very different fabric patterns within the ice-sheet, corresponding to different flow conditions. Strain-induced fabric, combined with the strong anisotropy of the crystal, result in a strong fabric-dependent anisotropy of the polycrystalline ice. As shown experimentally by Pimienta and others [78], a polycrystal of ice with all the c-axes of its grains orientated in the same direction deforms ten times faster than an equivalent isotropic sample, when it is sheared parallel to the basal planes.

The spatial variability of the observed fabrics, from single maximum fabrics [23, 88] to girdle type fabrics [58], indicates the strong coupling existing between the fabric and the local flow conditions. At some stage, it is a chance, because ice-sheets can be seen as a huge database containing fabric evolution experiments for a very large range of strain-history and temperature conditions. On the reverse, the very small amount of data (few ice cores) regarding the ice-sheets typical size renders the exploitation of all these data very difficult. Moreover, the very small strain-rates and very low temperatures prevailing inside an ice-sheet are quasi-impossible to be reproduced by cold-room experiments of fabric evolution. All these together clearly indicate that a strong modelling effort is needed in order to analyse the measured fabrics at a particular drilling site. Due to the complex coupling between the anisotropic flow and the fabric evolution, this modelling effort should include the coupling of both in a local flow model.

Very often, ice is assumed to be an isotropic medium, the behaviour of which follows a classical Norton-Hoff type law, namely the Glen's law in glaciology, linking the strain rate $\bar{\boldsymbol{D}}$ to the deviatoric Cauchy stress $\bar{\boldsymbol{S}}$:

$$\bar{\boldsymbol{D}} = \frac{B_n}{2}\tau^{n-1}\bar{\boldsymbol{S}}\,, \tag{1}$$

where $\tau^2 = \operatorname{tr}\bar{\boldsymbol{S}}^2/2$ is the second invariant of the deviatoric Cauchy stress and B_n is a fluidity parameter function of the temperature. The stress exponent entering the Glen's law is found to be close to 3 for laboratory experiments [26], whereas an exponent equal or even smaller than 2 is certainly more adapted to describe the behaviour of in-situ polycrystalline ice in the main part of the ice-sheets [19, 59, 61]. Within an ice-sheet, a stress exponent equal to 3 would be associated with deformation occurring in the bottom part of some cores, where the temperature can be higher than -10 °C and where dynamic migration[1] recrystallization is assumed to be

[1] Also called dynamic discontinuous recrystallization.

the main softening mechanism.

As far as the polycrystalline ice is textured, the Glen's law does not hold anymore, and an anisotropic formulation must be adopted to describe properly the polycrystalline anisotropic behaviour. The aim of this paper is to present the different classes of anisotropic models used so far in glaciology.

We first recall the deformation and recrystallization processes of polar ice. Then, the three existing models for the crystal are presented as well as the equations for crystal rotation. The different fabric descriptors are reviewed, and general relation linking these descriptors are given. A special emphasis is given to the comparison of the different parameterized orientation distribution functions presented in the glaciological literature so far. The various classes of anisotropic polycrystal models are then presented. At last, the existing anisotropic flow models and the results obtained from their applications are discussed.

2 Deformation and recrystallization processes of polar ice

2.1 Deformation mechanisms

When an ice core is located at a dome, a first order approximation is to assume a uniform steady-state vertical strain-rate $\dot{\epsilon}_{zz}$ along the core, given by:

$$\dot{\epsilon}_{zz} = b/H\,, \tag{2}$$

where b is the accumulation rate and H is the ice thickness. By taking values from Vostok (Antarctica) ice core, with the present accumulation rate of 2.3 g cm^{-2} a^{-1}, the vertical strain-rate is about 7×10^{-6} a^{-1} [58]. Lipenkov and others [58] estimated the horizontal shear strain-rate along Vostok ice core by assuming a flow law with a stress exponent n=3. With a surface slope of 10^{-3}, the horizontal shear stress at 2000 m depth is lower than 0.02 MPa, leading to a shear strain-rate of the order of 4×10^{-6} a^{-1} at the same depth.

Although strain-rates and deviatoric stresses are very low, it is now commonly accepted that deformation processes along polar ice cores are dominated by the viscoplastic mechanism of dislocation glide mainly along the basal plane. Diffusional creep, commonly associated with such conditions in many materials, yields a viscosity much higher than that deduced from field data [61]. Deformation by basal glide of dislocations is associated with efficient processes of accommodation such as normal grain growth and dynamic recrystallization which are described in the next paragraph.

2.2 Grain growth and recrystallization in ice-sheets

From texture and microstructure measurements along polar ice cores, it was evidenced that the evolution of ice structure is mainly associated with deformation processes but influenced by grain growth and recrystallization mechanisms [2, 8, 58]. Normal grain growth is distinctly observed in the upper layers of the ice sheets (several hundreds of meter) where the mean grain size is increasing with depth. Such a grain growth is driven by the decrease in free energy related to the reduction in grain boundary area. The grain size is generally larger than 1 mm and the grain boundary free energy is $\gamma_{gb} = 0.065$ J m^{-2} [3]. A parabolic growth relationship between grain size and time was found along several cores in Greenland and Antarctica [47, 58, 88].

Below this normal grain growth region, heterogeneous deformation within grains leads to localized high internal stresses that can relax through the formation of sub-boundaries, by the gathering of dislocations [3]. The misorientation associated with these sub-boundaries is supposed to increase with deformation and sub-boundaries to evolve into high-angle boundaries, leading to the creation of new grains (polygonization). Such a mechanism can be associated with grain boundary migration driven by the difference in deformation stored energy between boundaries and is named *rotation* or *continuous recrystallization*, but also with normal grain growth if the corresponding driving force remains higher (very low strain-rate conditions). Evidences of polygonization are given by the visualisation of low angle boundaries on ice thin sections, and the measurement of an average constant grain size along cores where temperature and impurity contents remain constant. For the Byrd ice core (Antarctica), Alley and others [4] indicate that polygonization processes associated with rotation recrystallization counteract further normal grain growth below 400 m depth. The same explanation was given [13, 88] for the constant average grain size measured along the GRIP ice core (Greenland) between 650 and 1500 m depth. Along the Vostok and EPICA Dome C ice cores (Antarctica), due to the continuous increase in temperature from the surface, such an interruption in the grain size profile is not observed.

Nevertheless, as shown along the EPICA Dome C ice core by Durand and others [24], the grain size variations along the main part of the core can only be well reproduced by modelling the effect of normal grain growth and rotation recrystallization, associated with the impact of impurity contents on the grain boundary migration rate. The pinning of grain boundaries by dust (insoluble impurities) explains most of the observed modifications of the microstructure, which are highly visible at the transition between glacial ice and interglacial ice, but rotation recrystallization becomes very active to balance normal grain growth in the range $1000 - 1750$ m. Below this depth, Durand and others [24] suggest a thermally activated unpinning of grain boundaries from particles and provide a good estimation of the average grain size evolution up to 2135 m.

More recently, Obbard and others have measured ori-

entation relations between neighbouring grains in ice from the GISP2 ice core (Greenland) [75] and the Vostok ice core [74], using the electron backscatter diffraction technique. Such a technique provides full $\boldsymbol{c}$- and $\boldsymbol{a}$-axis orientation of individual grains, and then allows to compare nearest-neighbour orientation relationships. Along both cores they measured correlations between adjacent grains that reveal the presence of polygonization associated with rotation recrystallization.

Deeper in some ice cores, very large amplitudes of grain size variations can be measured, such as below 2780 m along the GRIP core. Such high variations are attributed to the effect of a temperature increase in the core which can become higher than -10 °C, and favour the occurrence of migration recrystallization. This recrystallization process is characterised by a very fast grain growth, with a boundary velocity that can be 10 times higher than in the normal grain growth regime [27]. Such a recrystallization process is associated with the nucleation of new grains through a process that should be close to the bulging described for geological materials [48]. Migration recrystallization fabrics differ completely from strain-induced fabrics because the new grains are orientated favourably for the macroscopic deformation. Gow and Williamson [47] have reported similar observations on the lower part of the Byrd ice core.

2.3 Fabric development

In polar ice, the fabric is measured via the orientation of the grain c-axes [8, 58, 88, 92]. The fabric development as observed along polar ice cores is mainly associated with the rotation of grains induced by deformation, meaning by intracrystalline glide of dislocations, but can be influenced by recrystallization processes [3, 6, 17].

In the main part of the ice core, only normal grain growth and rotation recrystallization can influence fabric development. The exact influence on the c-axis rotation rate is not clear yet, although the observed fabrics in the corresponding part of the core are generally very close to what is expected considering the main imposed strain. Along the EPICA Dome C ice core, the strain is mainly vertical compression, due to the location of the core theoretically at a topographical dome. Such a main strain induces a rotation of the c-axes toward the vertical axis [21, 92]. This configuration was also observed along the GRIP and the Dome Fuji ice cores [7, 88]. Along the Vostok ice core, the main strain is horizontal tension, leading the c-axes to orientate in a vertical plane, perpendicular to the tension direction [58].

Nevertheless, texture observations (grain shape and orientation) reveal some areas where horizontal shear seems to have a noticeable effect [22, 21]. Such a shear will induce a sharp change in the texture development, by accelerating the rotation toward the vertical axis. As it will be discussed in the application part of this paper, such a shear can have a strong impact on ice flow, by inducing a positive feedback in some initially softer layers [21].

Although rotation recrystallization is only supposed to slow down the fabric development induced by the deformation, migration recrystallization induces fabrics which are much different than deformation-induced fabrics. As observed in alpine glaciers [61, 90], during lab experiments [51, 52] or at the bottom of the GRIP core [88], the c-axes are rotating toward a direction of easy glide, between 30° and 45° from the vertical axis. Such a fabric provides orientations that are favouring the imposed compression strain. The so-formed fabrics are either imposed by the nucleation of so-called *well* oriented grains, and/or the favoured growth of such grains. They are, then, controlled by the stress state within the polycrystal [25]. The induced softening of the polycrystal behaviour in the bottom part of the core can have a non-negligible impact on the global flow around the core, and should be accurately taken into account in modelling.

3 Models for the ice single crystal

3.1 Crystal viscous laws

Such models are required by homogenization models to derive the macroscopic behaviour from the microscopic properties. We present hereafter the three different approaches that can be found in the glaciological literature.

3.1.1 Schmid law

The classical approach in material science to describe the viscoplastic behaviour of a crystallite is the use of the so-called Schmid law, which consist of the sum of all the slip system contributions [9, 11, 12, 13]. To define the orientation of all these slip systems, one can introduce the Schmid tensor:

$$\boldsymbol{r}^s = \frac{1}{2}(\boldsymbol{n}^s \otimes \boldsymbol{b}^s + \boldsymbol{b}^s \otimes \boldsymbol{n}^s)\,, \tag{3}$$

where $\boldsymbol{n}^s$ and $\boldsymbol{b}^s$ are the unit vectors normal and parallel to the Burgers vector of the slip system s, respectively. For a given deviatoric Cauchy stress $\boldsymbol{S}$, the strain-rate $\boldsymbol{D}$ is obtained as:

$$\boldsymbol{D} = \left\{ \dot{\gamma}_0 \sum_{s=1}^{\mathcal{S}} \frac{\boldsymbol{r}^s \otimes \boldsymbol{r}^s}{\tau_0^s} \left| \frac{\boldsymbol{r}^s : \boldsymbol{S}}{\tau_0^s} \right|^{n-1} \right\} : \boldsymbol{S}\,, \tag{4}$$

where $\dot{\gamma}_0$ is a reference shear rate and the τ_0^s are the reference resolved shear stresses (RRSS) which control the stiffness of each slip system. The stress sensitivity exponent n can be different for each slip system, but in practise the same value is always adopted. For ice, Castelnau and others [11] have numbered nine independent slip systems arising from the choice of the three families of

planes: basal (two independent systems), prismatic (two) and pyramidal (five). Due to the very strong anisotropy of the crystal, the RRSS for the basal plane τ_0^b is expected to be much larger than the prismatic and pyramidal ones (τ_0^{pr} and τ_0^{py}, respectively). In order to define the position of the slip systems relative to a fixed reference frame, the three Euler angles are needed.

3.1.2 Basal slip system model

Considering that most of the deformation of a single crystal results from basal glide and noticing that the basal plane is isotropic when $n = 1$ or $n = 3$ [53], many authors have adopted a simple model for the ice crystal assuming only deformation by basal glide [5, 10, 45, 60, 91]. When expressed in the grain reference frame $\{^g\mathsf{R}\}$ defined by $\boldsymbol{e}_3^g = \boldsymbol{c}$, this law simply reads:

$$D_{i3}^g = \frac{\psi_n}{2} \tau_b^{n-1} S_{i3}^g \quad i = 1, 2\,, \tag{5}$$

where $\tau_b^2 = ({S_{13}^g}^2 + {S_{23}^g}^2)/2$, and ψ_n is the reference fluidity for basal glide. This simple law considers that all the other non-basal strain-rate components vanish. The main advantage of this law is its simplicity, and that only one orientation (two angles) is needed in order to orientate the grain relative to a fixed reference frame. On the other hand, the main drawback of this law is to conduct to zero deformation in some directions for strongly textured polycrystal (one maximum or girdle type fabrics).

3.1.3 Continuous Transversely Isotropic (CTI) model

With the idea of keeping the advantage of a grain orientated solely by one unit vector, while ameliorating the behaviour description of the previous model, Meyssonnier and Philip [67] have proposed a continuous transversely isotropic (CTI) law in the particular case of a linear behaviour ($n = 1$):

$$\begin{aligned} \boldsymbol{D} = & \frac{\psi_1}{2} \left(\beta \boldsymbol{S} + (1-\beta)(\boldsymbol{S}\cdot\boldsymbol{M}_3 + \boldsymbol{M}_3\cdot\boldsymbol{S})^D\right) \\ & + \psi_1 \beta \frac{\gamma+2}{4\gamma-1} \operatorname{tr}(\boldsymbol{M}_3\cdot\boldsymbol{S})\boldsymbol{M}_3^D\,, \end{aligned} \tag{6}$$

where $\boldsymbol{M}_3 = \boldsymbol{c}\otimes\boldsymbol{c}$ is the structure tensor used to describe the axial symmetry around the crystal $\boldsymbol{c}$ axis. The notation $()^D$ denotes the symmetric part of a tensor. The three introduced rheological parameters allow to quantify the crystal anisotropy: ψ_1 is the basal shear fluidity, β characterises the fluidity ratio in and parallel to the basal planes, and γ is the tension-compression fluidity ratio in and perpendicular to the basal planes. The strong crystal anisotropy and the condition that the dissipation potential must be positive, lead to the following inequalities: $0 \leq \beta << 1$ and $1/4 \leq \gamma \approx 1$. The extension to the non-linear case ($n \neq 1$) is not straightforward and has not been developed so far.

One can show that in the linear case, the Schmid law (4) and the CTI law (6) are fully equivalent, and the rheological parameters of one can be identified from those of the other [66]. Moreover, when considering only basal planes, by setting infinite RRSS in prismatic and pyramidal planes for the Schmid law (4) and $\beta = 0$ in the CTI law (6), the three presented crystal laws are equivalents.

3.2 Crystal rotation

The crystal deformation resulting from dislocation glide in the different slip planes induces an evolution of the orientation of these planes. For a large part of the ice-sheet, this rotation induced by deformation is the most important mechanism contributing to the fabric evolution. The rotation rate of the orientation of a crystal can be written as:

$$\dot{\boldsymbol{c}} = \boldsymbol{W}\cdot\boldsymbol{c} - \lambda[\boldsymbol{D}\cdot\boldsymbol{c} - (\boldsymbol{c}^T\cdot\boldsymbol{D}\cdot\boldsymbol{c})\boldsymbol{c}]\,, \tag{7}$$

where $\boldsymbol{W}$ and $\boldsymbol{D}$ are the spin and strain-rate on the grain, respectively [41] and λ is a parameter depending on the grain model. This relation indicates that the rotation of the grain's reference frame $\{^g\mathsf{R}\}$ (the term $\dot{\boldsymbol{c}}$) is equal to the total spin ($\boldsymbol{W}.\boldsymbol{c}$) minus the viscoplastic spin induced by deformation ($\lambda[\boldsymbol{D}.\boldsymbol{c} - (\boldsymbol{c}^T.\boldsymbol{D}.\boldsymbol{c})]$). This last term can be identified as the $\boldsymbol{c}$-axis spin relative to the crystal reference frame $\{^g\mathsf{R}\}$. For the basal plane model (5) and the CTI model (6), assuming that the grain rotation is solely induced by the glide in basal planes [67], the strain-rate and spin verify the following relation when expressed in $\{^g\mathsf{R}\}$:

$$W_{i3}^g = D_{i3}^g\,, \quad i = 1, 2\,, \tag{8}$$

which do correspond to $\lambda = 1$. This assumption, which assumes that the viscoplastic spin of the grain $\boldsymbol{c}$-axis is only due to the contribution of basal planes and neglects contributions of the prismatic and pyramidal planes is well-founded for polar ice and has been used in many models [5, 45, 60, 85, 86].

For the Schmid law model (4), grain rotation is the result of all contributions of the three considered planes, and one can show that it corresponds to $\lambda = (\tau_0^{py} + 2\chi\tau_0^b)/(\tau_0^{py} + 2\chi^2\tau_0^b) \leq 1$, where $\chi = [1 - (c/a)^2]/[1 + (c/a)^2]$ and $c/a = 1.629$ is the ratio of the crystal lattice dimensions [39].

When $\lambda = 1$, similarly to what was done by Dinh and Armstrong [18] for fiber material, one can show that the grain orientation at time t can be uniquely expressed as a function of its initial orientation $\boldsymbol{c}_0$ and the deformation gradient $\boldsymbol{F}$ ($F_{ij} = \partial x_i/\partial x_j^0$) undergone from t_0 to t, by:

$$\boldsymbol{c} = \frac{\boldsymbol{F}^{-T}\cdot\boldsymbol{c}_0}{(\boldsymbol{c}_0^T\cdot\boldsymbol{F}^{-1}\cdot\boldsymbol{F}^{-T}\cdot\boldsymbol{c}_0)^{1/2}}\,. \tag{9}$$

4 Fabric description

At the macroscopic scale, the anisotropic behaviour is strongly related to the distribution of the orientations of all the crystals which compose the polycrystal. The aim of this part is to review the possible methods to describe this distribution of orientations. With regard to other materials, most of the proposed methods take advantage of the crystal hexagonal symmetry which allows to orientate the ice crystal with only one unit vector.

4.1 Discrete description

The more natural way to describe the fabric of a polycrystal is to give the orientation and associated volume fraction f_k of a finite number of crystals N_g. For the orientation, the three Euler angles should be used in order to define with no ambiguity the crystal reference frame [11] relative to the polycrystal reference frame. Such a description is in fact only used when the crystal behaviour is inferred from the Schmid law, for which all the slip system are described. As shown in the previous section, in the linear case, the Schmid law is transversely isotropic and is identical to the CTI law presented in Section 3.1.3. When accounting only for the basal slip systems, the crystal behaviour is also transversely isotropic for both linear and non-linear ($n = 3$) behaviours. Therefore, for all these cases, only one orientation, *i.e.,* the $\boldsymbol{c}$-axis unit vector, is necessary to define the crystal position. The $\boldsymbol{c}$-axis orientation is generally defined by two angles using a spherical coordinate system, namely the longitude φ_k and the co-latitude θ_k. This feature is exploited to derive the continuous description presented in the next section.

For the volume fraction f_k, if the fabric is inferred from data measurements on thin sections, it should be estimated using the cross-sectional area of the grain as suggested by Gagliardini and others [34].

Using the discrete description for the fabric, a macroscopic quantity $\bar{Y}$ is determined as the average of the microscopic quantities Y_k over all the grains:

$$\bar{Y} =< Y_k >= \sum_{k=1}^{N_g} f_k Y_k(\boldsymbol{c}_k)\,, \tag{10}$$

and by definition $\sum_{k=1}^{N_g} f_k = 1$.

4.2 Continuous description

4.2.1 Orientation Distribution Function (ODF)

The Orientation Distribution Function (ODF) is a continuous, positive and infinitely differentiable function of the orientation. The probability P_k to find grain orientations within the solid angle $\mathrm{d}\boldsymbol{c}$ centred around the direction $\boldsymbol{c}$, which expresses the volume fraction $dV(\boldsymbol{c})/V_0$ of these grains, reads:

$$P_k = dV(\boldsymbol{c})/V_0 = \frac{1}{2\pi} f(\boldsymbol{c})\,\mathrm{d}\boldsymbol{c}\,. \tag{11}$$

By definition, this implies

$$\frac{1}{2\pi} \oint_{S/2} f(\boldsymbol{c})\,\mathrm{d}\boldsymbol{c} = 1. \tag{12}$$

This volume fraction reduces to a relative number of grains only in the very idealised case where all the grains have the same volume. In practice, the ODF $f(\boldsymbol{c})$ itself can be seen as the density of orientations over the half unit sphere, because common practice is to set $f(\boldsymbol{c}) = 1$ for a uniform distribution of orientations.

Since it is not possible to distinguish a grain with an orientation $\boldsymbol{c}$ from a grain with an orientation $-\boldsymbol{c}$, the space of all possible orientations is the half unit sphere $S/2$ or, using the spherical coordinate system, $\theta \times \varphi \in [0, \pi/2] \times [0, 2\pi]$.

When using an ODF, the volume average of a microscopic quantity $Y(\boldsymbol{c})$ is given as:

$$\bar{Y} =< Y(\boldsymbol{c}) >= \frac{1}{2\pi} \oint_{S/2} f(\boldsymbol{c}) Y(\boldsymbol{c})\,\mathrm{d}\boldsymbol{c}\,. \tag{13}$$

4.2.2 Orientation tensors

The orientation tensors are defined as the different moments of the ODF:

$$\boldsymbol{a}^{(p)} =< \boldsymbol{c} \otimes \underbrace{\boldsymbol{c} \otimes \ldots}_{p-2} \boldsymbol{c} > \,, \tag{14}$$

where the average $< . >$ is either given by (10) for a discrete description of the fabric or by (13) for a continuous description. Consequently, the orientation tensors allow an objective comparison of these two different fabric descriptions.

By analogy with the inertial products which characterise the mass repartition over a unit sphere, the orientation tensors characterise the repartition of the c-axis intersections with the unit sphere of orientation.

The second-order orientation tensor $\boldsymbol{a}^{(2)}$ is now commonly used to describe the measured fabrics [20, 88, 93, 92]. It gives a more pertinent information than the older parameters like the strength of the fabric or the spherical aperture [20]. The eigenvalues of $\boldsymbol{a}^{(2)}$ are related to the spatial strength of the fabric, whereas the eigenvectors give the disorientation of the maximum strengths relative to a reference frame. The eigenvectors are often assimilated as the *best* material symmetry basis. Since by definition $\mathrm{tr}\,\boldsymbol{a}^{(2)} = 1$ and the orientation tensors are symmetric, only 5 components of $\boldsymbol{a}^{(2)}$ are independent. The different observed fabrics can be classified as a function of the values of the eigenvalues:
- $a_1^{(2)} \approx a_2^{(2)} \approx a_3^{(2)} \approx 1/3$ for an isotropic fabric,
- $1 \geq a_1^{(2)} > 1/3 > a_2^{(2)} \approx a_3^{(2)} \geq 0$ for a single maximum fabric,
- $1 > a_1^{(2)} \approx a_2^{(2)} > 1/3 > a_3^{(2)} \geq 0$ for a girdle fabric,
- $1 > a_1^{(2)} > a_2^{(2)} > a_3^{(2)} > 0$ for more general fabric patterns.

Two different fabrics (different distributions of grain orientations) can have the same $\boldsymbol{a}^{(2)}$, but the higher even order orientation tensors will be different, and consequently these two fabric samples should behave slightly differently. In the reverse, $\boldsymbol{a}^{(4)}$ contains all the fabric information included in $\boldsymbol{a}^{(2)}$; for example:

$$a^{(2)}_{ij} = a^{(4)}_{ij11} + a^{(4)}_{ij22} + a^{(4)}_{ij33}\,. \tag{15}$$

On the other hand, the second order orientation tensor is also used as a fabric parameter to describe the fabric in polycrystal models [41, 44]. In Section 5.1, an analytical derivation of the polycrystal behaviour is inferred for the uniform stress model using the orientation tensors to describe the fabric.

4.2.3 Link between ODF and orientation tensors

As shown by Zheng and Zou [94], the ODF can be expressed as a tensorial expansion of the even order orientation tensors. For the two first terms, this expansion takes the form:

$$\begin{aligned} f(\boldsymbol{c}) = 1 &+ \frac{15}{2}\llcorner \boldsymbol{a}^{(2)} \lrcorner : \boldsymbol{c}\otimes\boldsymbol{c} \\ &+ \frac{315}{8}\llcorner \boldsymbol{a}^{(4)} \lrcorner :: \boldsymbol{c}\otimes\boldsymbol{c}\otimes\boldsymbol{c}\otimes\boldsymbol{c} + \dots\,, \end{aligned} \tag{16}$$

where $\llcorner \boldsymbol{a}^{(n)} \lrcorner$ denotes the irreducible part[2] of the tensor $\boldsymbol{a}^{(n)}$. From (16), the link between the eigenvalues of $\boldsymbol{a}^{(2)}$ and the ODF becomes clear: when expressed in the principal reference frame, the ODF constructed from (16) up to $\boldsymbol{a}^{(2)}$ is an ellipsoid, length axis of which in direction i is proportional to $a^{(2)}_i$. As an example, the contribution of the different terms of the tensorial expansion (16) is plotted in Figure 1 for a plane isotropic fabric and a plane bi-axial fabric. Obviously these two fabrics have the same second order orientation tensor ($a^{(2)}_{11} = a^{(2)}_{22} = 1/2$ and other components zero), so that the ODF is identical up to the second-order orientation tensor expansion, while the contribution from the fourth-order orientation tensors are different.

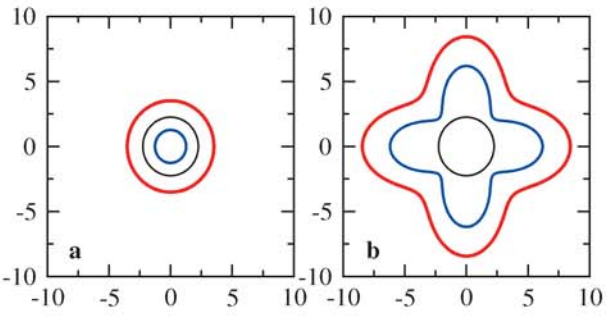

Figure 1: *Section in the planes* 1 *and* 2 *of the ODF (16) for* **(a)** *a plane isotropic fabric (*$\boldsymbol{c}$*-axis randomly distributed in a plane) and* **(b)** *a plane bi-axial fabric (half* $\boldsymbol{c}$*-axis horizontal and half vertical). The thin black line shows the contribution of* $\boldsymbol{a}^{(2)}$*, the thick blue line the contribution of* $\boldsymbol{a}^{(4)}$ *and the thick red line indicates the contribution from both* $\boldsymbol{a}^{(2)}$ *and* $\boldsymbol{a}^{(4)}$*.*

4.2.4 Analytical ODF

By definition, for the uniform strain-rate model (see Section 5.1), each grain experiences the same deformation gradient tensor, which is equal to the macroscopic deformation gradient experienced by the ice polycrystal $\bar{\boldsymbol{F}}$, defined by

$$\bar{F}_{ij} = \frac{\partial \bar{x}_i}{\partial \bar{x}^0_j} \quad \text{and} \quad \dot{\bar{\boldsymbol{F}}} = \bar{\boldsymbol{L}}\cdot\bar{\boldsymbol{F}}\,, \tag{17}$$

where $\bar{x}_i$ and $\bar{x}^0_i$ are the coordinates at time t and t^0 respectively.

Following Dinh and Armstrong [18], if the ice fabric is isotropic at time t^0, i.e. $f \equiv 1$, then we can check that

$$f(\boldsymbol{c}) = (\boldsymbol{c}^T\cdot\bar{\boldsymbol{F}}\cdot\bar{\boldsymbol{F}}^T\cdot\boldsymbol{c})^{-3/2} \tag{18}$$

is a solution of the equation for the evolution of the ODF (36) for the uniform strain-rate model (see its definition in Section 5.1), with the $\boldsymbol{c}-$axis rotation velocity given by (7) assuming $\lambda = 1$. The ODF is then only a function of the deformation gradient experienced by the ice polycrystal $\bar{\boldsymbol{F}}$, which is a solution of the linear equation $(17)_2$, and which exhibits analytical solutions for several flow conditions. The generic expression (18) should have been used to derive the more specific ones obtained later and restricted to some particular loading conditions, as in [35, 43, 45, 46, 85].

As an example, the analytical expression for a simple shear solicitation, defined by $F_{11} = F_{22} = F_{33} = 1$, $F_{12} = \kappa$ and other terms zero, is obtained directly from (18) as:

$$f = (\cos^2\theta + \sin^2\theta(\cos^2\varphi + (\sin\varphi + \kappa\cos\varphi)^2))^{-3/2}\,. \tag{19}$$

Similar analytical solution can also be derived under the static assumption (uniform stress, see Section 5.1), but for less general loading conditions [35, 43].

4.2.5 Parameterized ODF

From heuristic considerations or using the previous analytical solutions, some parameterized ODF (PODF) have been proposed in order to decrease the number of parameters needed to describe the fabric. In this section, these PODF are presented and compared.

Lliboutry [60] has proposed to use a Fisherian distribution:

$$f_k(\theta) = \frac{k\,\mathrm{e}^{k\cos\theta}}{\mathrm{e}^k - 1}\,, \tag{20}$$

but finally adopted the following PODF:

$$f_\nu(\theta) = \nu\cos^{\nu-1}\theta\,. \tag{21}$$

[2]For the second order orientation tensor, $\llcorner \boldsymbol{a}^{(2)} \lrcorner = \boldsymbol{a}^{(2)} - \boldsymbol{I}/3$, where $\boldsymbol{I}$ is the identity tensor; more details can be found in [39], page 36.

Meyssonnier and Philip [67] used a discretized ODF over 90 intervals between 0 and $\pi/2$. They showed that the discretized ODF can be very accurately fitted using the following PODF:

$$f_{q_i}(\theta) = \left[q_0 + q_1 \cos 2\theta + q_2 \cos^2 2\theta\right]^{-1}. \qquad (22)$$

From an analytical solution, Gödert [43] has derived a semi-parameterized ODF restricted to planar flow. Assuming that the direction 3 is the direction perpendicular to the plane flow, the proposed PODF takes the form:

$$f_{a,b,c}(\theta,\varphi) = [\lambda^{-2/3}\cos^2\theta + (a + b\sin 2\varphi + c\cos 2\varphi)\lambda^{1/3}\sin^2\theta]^{-3/2}, \qquad (23)$$

where $\lambda = \mathrm{e}^{-3\sum \Delta t D_{33}}$. In (23), only the in-plane form of the fabric is parameterized since the concentration perpendicular to the plane flow is given analytically as a function of the strain-rate normal to the plane flow (D_{33}).

Using the same analytical approach [35], Gagliardini and Meyssonnier have proposed a PODF for an orthotropic fabric [36]:

$$f_{k_1,k_2,\varphi_0}(\theta,\varphi) = [(k_1k_2)^{-2}\cos^2\theta + \sin^2\theta(k_1^2\cos^2(\varphi-\varphi_0) + k_2^2\sin^2(\varphi-\varphi_0))]^{-3/2}. \qquad (24)$$

The two parameters k_1 and k_2 control the fabric strength, whereas φ_0 gives the inclination of the material symmetry reference frame in the particular case of planar flow.

PODF (23) and (24) lead to exactly the same orientation distribution since analytical relations[3] can be obtained between the two sets of parameters (k_1, k_2, φ_0) and (a, b, c, λ). Using the conservation equation (12) in (23), one of the four parameters can be expressed as a function of the three others: $a = (b^2/\sin(\arctan(b/c))^2 - 1)^{1/2}$.

Noticing that most of the observed fabrics have a vertical axis of rotational symmetry, Thorsteinsson [86] built his PODF by assuming a uniform distribution within the two angles α_0 and α, such that:

$$f_{\alpha_0,\alpha}(\theta) = \frac{1}{\cos\alpha_0 - \cos\alpha}, 0 \le \alpha_0 \le \theta \le \alpha \le \frac{\pi}{2}. \qquad (25)$$

More recently, Placidi and Hutter [79] have adopted the following PODF:

$$f_{\theta_0}(\theta) = \frac{\delta(\theta-\theta_0)}{\sin\theta_0}, \qquad (26)$$

where δ denotes the Dirac function.

Except for (23) and (24), all the other PODF found in the literature are restricted to a fabric which shows a rotational symmetry. Since all these PODF are expressed in the material symmetry reference frame of the polycrystal, two Euler angles have to be added to the set of parameters to give the position of the fabric symmetry axis relative to a general reference frame. The PODF (23) and (24) include the orientation of one of the axes of the material symmetry reference frame, and are restricted to the particular case of a planar flow. For more complex flow, one should for example set $\varphi_0 = 0$ in (24) and use three Euler angles to fix the material symmetry reference frame relative to a general reference frame.

Except for (22) and (23), all the other PODF fulfil implicitly the total volume conservation (12). No simple relation was found for the three parameters in (22) in order to express one of the parameters as a function of the two others. As a consequence, neither combination of the three parameters q_i in (22) guarantees that the volume conservation is fulfilled. This condition must be verified afterwards, which in reality render the use of this PODF very complicated.

Except for (26), all the presented PODF reduce to the expected value $f = 1$ for isotropic ice.

As presented in the previous section, the orientation tensors allow an objective comparison of fabrics. Assuming a transversely isotropic fabric around $\boldsymbol{e}_3$, *i.e.* $a_{33}^{(2)} = 1 - 2a_{11}^{(2)}$, $a_{11}^{(2)} = a_{22}^{(2)}$ and $a_{ij} = 0$ if $i \neq j$, one can compare the different PODF for a given $a_{33}^{(2)}$. The relation between the PODF parameter(s) p and $a_{33}^{(2)}$ is given by:

$$a_{33}^{(2)} = \int_0^{\pi/2} f_p(\theta)\cos^2\theta\sin\theta\,\mathrm{d}\theta, \qquad (27)$$

and therefore $a_{33}^{(2)} = [(k^2-2k+2)\,\mathrm{e}^k - 2]/[(k^2(\mathrm{e}^k-1)]$ and $a_{33}^{(2)} = \nu/(\nu+2)$ for Lliboutry's PODF (20) and (21), respectively, $a_{33}^{(2)} = (\cos^2\alpha_0 + \cos\alpha_0\cos\alpha + \cos^2\alpha)/3$ for Thorsteinsson's PODF (25) and $a_{33}^{(2)} = \cos^2\theta_0$ for Placidi and Hutter's PODF (26). In the case of a transversely isotropic fabric, $k_1 = k_2$, and the Gagliardini and Meyssonnier's PODF (24), as well as the Gödert's PODF, is only a function of θ. Following [35], an analytical relation can be derived between $a_{33}^{(2)}$ and the PODF parameter k_1 (from equations (40), (42) and (43) in [35]).

Since the Thorsteinsson's PODF (25) depends on two parameters, for a given value of $a_{33}^{(2)}$, the choice of these two parameters is not unique. As done by Thorsteinsson [86], one can adopt $\alpha_0 = 0$ for single maximum fabrics (cone fabrics), but as far as $a_{33}^{(2)} < 1/3$ (girdle fabric), the parameters must verify $\alpha_0 \ge \arccos(3a_{33}^{(2)})^{1/2}$ and $\alpha = \pi/2$.

All these PODF, as well as measured ODF, are compared in Figure 2. Obviously, the Fisherian distribution proposed by Lliboutry [60], which has never been applied in glaciology, fits best the observed distribution of grain orientations. PODF (25) and (26) give unrealistic distributions whereas PODF (22), (23) and (24) lead to a

[3] $2\varphi_0 = \arctan(b/c)$, $k_1^2 = \lambda^{1/3}(a + b/\sin 2\varphi_0)$ and $k_2^2 = \lambda^{1/3}(a - b/\sin 2\varphi_0)$.

too much concentrated fabric. Since the PODF (23) and (24) were derived from an analytical solution assuming that the grain rotation is only the result of the glide of dislocations along the crystallographic planes, the difference between the measured fabrics and the PODF (23) and (24) might be explained by the rotation recrystallization which has the effect of decreasing the fabric strength in compression.

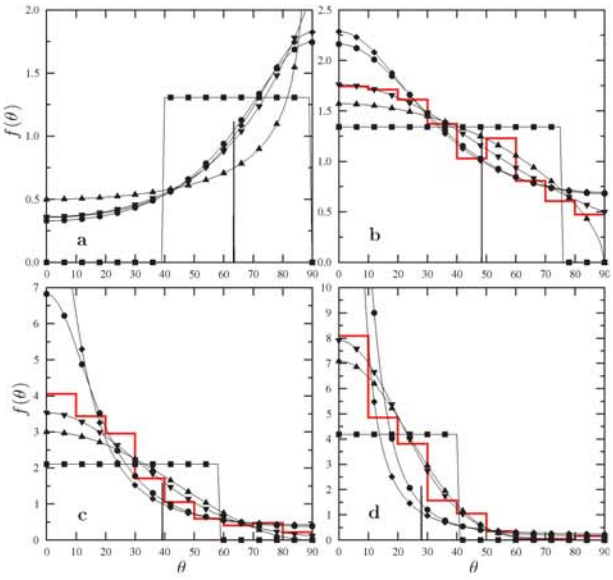

Figure 2: *Comparison of the different PODF -▼-(20), -▲-(21), -♦-(22) , -●-(23) and (24), -■-(25) and -no symbol-(26) for* **(a)** $a_{33}^{(2)} = 0.20$, **(b)** $a_{33}^{(2)} = 0.44$, **(c)** $a_{33}^{(2)} = 0.60$ *and* **(d)** $a_{33}^{(2)} = 0.78$. *The thick red curve represents measurements from the Dome C core for the same value of* $a_{33}^{(2)}$ *and* $a_{11}^{(2)} \approx a_{22}^{(2)}$ *(G. Durand, personal communication).*

The choice of a PODF implicitly determines all the even order orientation tensors. Even if for a particular value of the parameter(s) of the PODF, one can obtain the same second-order orientation tensor, the higher order orientation tensors will be different (else the PODF curves in Figure 2 would be superimposed). Therefore, even for the same second-order orientation tensor and the same homogenization model, the polycrystal response should be different for all these PODF.

In order to compare the difference in terms of polycrystal behaviour induced by these differences in the distribution of orientations, the enhancements in shear E^{cis} and in compression E^{co} relative to isotropic ice are plotted in Figure 3 as a function of $a_{33}^{(2)}$. For all the PODF, the same grain behaviour (CTI law (6) with $\beta = 0.01$ and $\gamma = 1$) and the same homogenization model (uniform stress model from Equation (29) in Section 5.1) have been used. Because in the linear case the polycrystal behaviour depends only on the second and fourth order orientation tensors, the observed differences are only due to differences in the fourth-order orientation tensor. Moreover, for axisymmetric fabrics, E^{cis} and E^{co} depend only on $a_{1122}^{(4)}$. For perfect girdle ($a_{33}^{(2)} = 0$), isotropic ($a_{33}^{(2)} = 1/3$) and perfect single maximum ($a_{33}^{(2)} = 1$) fabrics, the same values for $a_{1122}^{(4)}$ ($a_{1122}^{(4)} = 1/8,\ 1/15$ and 0, respectively) are obtained for all the PODF, except for (26). The maximum relative difference between all the PODF (excluding (26)) is about 20% for E^{cis} with $a_{33}^{(2)} = 0.5$ and up to 125% for E^{co} with $a_{33}^{(2)} = 0.6$. As expected in compression, for all the PODF the ice is easier to deform ($E^{co} > 1$) for $1/3 < a_{33}^{(2)} < a_{33limit}^{(2)}$, and for more concentrated fabrics, the ice becomes harder to deform. As shown in Figure 3**c**, the value of $a_{33limit}^{(2)}$, for which E^{co} is equal to one again, varies from 0.54 for the Meyssonnier's PODF (22) up to 0.85 for the Thorsteinsson's PODF (25).

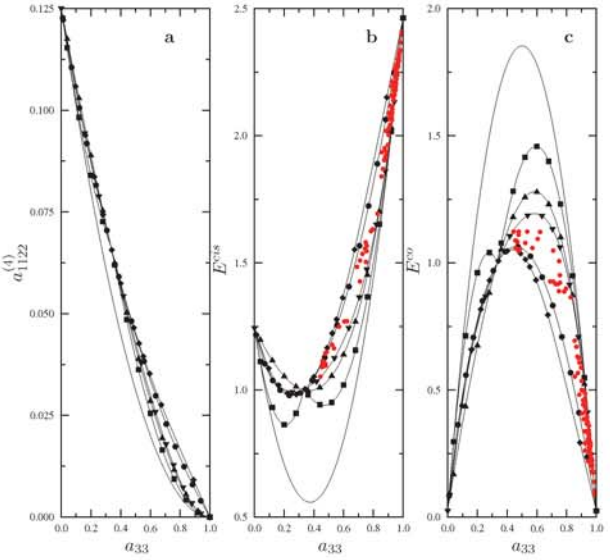

Figure 3: *Evolution of* **(a)** $a_{1122}^{(4)}$, **(b)** E^{cis} *and* **(c)** E^{co} *as a function of* $a_{33}^{(2)}$ *for the different PODF -▼-(20), -▲-(21), -♦-(22), -●-(23) and (24), -■-(25) and -no symbol-(26). Red circles represent enhancement factors for some of the measured Dome C fabrics (G. Durand, personnal communication). Enhancements in shear* E^{cis} *and in compression* E^{co} *relative to isotropy have been calculated using the static model and a grain anisotropy given by* $\beta = 0.01$ *and* $\gamma = 1$.

These differences might be larger for a non-linear behaviour because the polycrystal law will depend on the first four even orientation tensors (when $n = 3$).

5 Polycrystal models

5.1 Homogenization models

The concept of homogenization models, also called micro-macro models or volume fraction models, is to derive the polycrystal behaviour from the crystal one and the fabric. The fabric description can contain topological information to take into account neighbour influence (see Section 5.1.3), but generally it is only given as an orientation distribution, either discrete (Section 4.1) or continuous (Section 4.2).

The difference between all the homogenization models comes from their formulations and the hypotheses, implicit or explicit, used to take into account the grain-to-grain interaction.

For all these models, the macroscopic strain-rate $\bar{\boldsymbol{D}}$ and the macroscopic deviatoric stress $\bar{\boldsymbol{S}}$ are evaluated as the average of the strain-rate and deviatoric stress, respectively, over all the grains that compose the polycrystal:

$$\bar{\boldsymbol{D}} = < \boldsymbol{D} > \quad \text{and} \quad \bar{\boldsymbol{S}} = < \boldsymbol{S} > \,. \tag{28}$$

The average $< . >$ is either defined by (10) for a discrete description of the fabric or by (13) for a continuous one.

5.1.1 Static and Taylor bounds

The Taylor model assumes a uniform strain-rate distribution over all the grains, so that the strain-rate experienced by a grain is the same as that experienced by the polycrystal considered as a homogeneous medium: $\boldsymbol{D} = \bar{\boldsymbol{D}}$. On the other side, the static model supposes a uniform stress distribution ($\boldsymbol{S} = \bar{\boldsymbol{S}}$). For a given applied strain-rate, the static and Taylor models provide the lower and upper bounds, respectively, for the dissipation potential [54].

Due to the strong crystal anisotropy, the static model has been shown to be well adapted to describe the polycrystalline ice behaviour, whereas it is the opposite for the Taylor model [11].

The static model has been often used either with a discrete description of the fabric [10, 91] or a continuum description [35, 45, 60, 85], mainly because it allows analytical developments. Using either the CTI law (5) or (6) and the orientation tensor to describe the fabric, analytical expressions for the static model can be derived easily. As an example, this expression using the CTI law (6) with $\gamma = 1$, simply reads:

$$\begin{aligned} \bar{\boldsymbol{D}} = \frac{\psi_1}{2} \left[\beta \bar{\boldsymbol{S}} + (1-\beta)(\boldsymbol{a}^{(2)} \cdot \bar{\boldsymbol{S}} + \bar{\boldsymbol{S}} \cdot \boldsymbol{a}^{(2)}) \right] \\ + \psi_1 (\beta - 1) \boldsymbol{a}^{(4)} : \bar{\boldsymbol{S}} \,. \end{aligned} \tag{29}$$

As shown by Equation (29), in the linear case, the macroscopic expression depends on the first two even order orientation tensors.

In the limit case of an isotropic fabric, the second and fourth order orientation tensors simply read $a^{(2)}_{ij} = \delta_{ij}/3$ and $a^{(4)}_{ijkl} = (\delta_{ij}\delta_{kl} + \delta_{ik}\delta_{jl} + \delta_{il}\delta_{jk})/15$ $(i,j,k,l = 1,2,3)$. The static law (29) reduces then to the isotropic Glen's law (1), and the following relation between the grain parameters[4] ψ_1, β and γ, and the macroscopic Glen's law fluidity B_1 is obtained:

$$\frac{\psi_1}{B_1} = 5 \frac{4\gamma - 1}{8\gamma(\beta+1) + \beta - 2} \,. \tag{30}$$

For a one-site model, the grain-to-grain interaction is not taken into account, so that the behaviour of a polycrystal with a single maximum fabric is fully equivalent to that of the single crystal. Therefore, the grain parameters should be identified, not regarding the crystal behaviour, but from experimental tests on a polycrystal with a strong single maximum fabric. Experimentally, it is then found that such a polycrystal is approximately 10 times easier to shear perpendicular to the mean $\boldsymbol{c}$-axis orientation than a polycrystal with an isotropic fabric [78]. The ratio $\psi_1/B_1 = 10$ can then be used to select the parameters (β, γ). For the static model, the maximum value for this ratio is $5/2$ in the linear case and $35/8 = 4.375$ when $n = 3$ [60]. The experimental ratio of 10 is then not reached by the static model, and this is the main drawback of this model. With the static model, the anisotropy enhancement of the flow is always underestimated for single maximum fabrics by a factor 4 in the linear case and greater than 2 when $n = 3$. The use of intermediate models, as presented below, allows to avoid this drawback.

5.1.2 Visco-Plastic Self-Consistent (VPSC) model

The VPSC model has been adapted to ice by Castelnau and others [11] using a discrete description of the fabric. As shown by Castelnau and others [12] from mechanical tests on GRIP (Greenland) ice specimens, this model reproduces adequately the dependence of the ice rheology on its fabric. The VPSC model is a so-called *one-site approximation* in which the influence of the neighbourhood of each grain is accounted for by considering this grain as an inclusion embedded in a homogeneous matrix, the so-called *homogeneous equivalent medium* (HEM). The HEM behaviour, which represents that of the polycrystal, is to be determined. The basis of the VPSC homogenization scheme is the local *interaction formula* that provides a relation between the local stress and the local strain-rate acting on a grain (different from grain to grain) and the corresponding macroscopic quantities. It is written as

$$\boldsymbol{D} - \bar{\boldsymbol{D}} = -\tilde{\boldsymbol{M}} : (\boldsymbol{S} - \bar{\boldsymbol{S}}) \,, \tag{31}$$

where the interaction tensor $\tilde{\boldsymbol{M}}$ is a function of the grain and of the (unknown) HEM mechanical properties (see Equations (17-19) in [11] for details). By construction, if the same stress sensitivity exponent is adopted for all the crystallographic planes, then the HEM and the grain will have the same exponent. The macroscopic behaviour of the HEM is obtained by solving the equation $\bar{\boldsymbol{D}} = < \boldsymbol{D} >$.

To solve this equation, Castelnau and others used the averaging formula (10) and the Schmid law (4) with a stress exponent $n = 3$. In the non-linear case, the results are strongly dependent on the linearisation of the local behaviour, leading to the so-called *secant*, *tangent* and *affine* formulations; however, Castelnau and others used only the tangent formulation [9]. The above assumption may be questionable for ice, where a strong directionality and large variations in local properties are expected.

[4] Formally, to obtain relation (30), one should derive an expression similar to (29) without assuming $\gamma = 1$.

Furthermore, the tangent formulation was shown to saturate for high anisotropy [42]. The non-dependence with higher-order statistical moments is particularly critical for the treatment of those highly-contrasted materials, since such information is essential to capture, in an average sense, the effect of the strong strain-rate gradients that are likely to develop inside grains which are highly anisotropic. In order to overcome the above limitations, Lebensohn and others have applied to ice a rigorous nonlinear homogenization scheme, the *second-order* VPSC model, that takes into account information on the average field fluctuations at the grain level [56]. Among the various nonlinear extensions of the self-consistent approximation, the *second-order* method gives the best overall agreement with the effective properties and field fluctuations obtained by means of full-field simulations (see below), for both 2-D and 3-D polycrystals [56].

In the linear case, there is only one formulation for the VPSC model, and the macroscopic behaviour of the HEM can be obtained by solving either the equation $\bar{\boldsymbol{D}} =< \boldsymbol{D} >$ or $\bar{\boldsymbol{S}} =< \boldsymbol{S} >$. Meyssonnier and Philip have derived a semi-analytical solution in this particular linear case, using the CTI model (6) with $\gamma = 1$ for the grain and an ODF with transverse symmetries to describe the fabric [67].

When using the VPSC model it is not possible to achieve the HEM behaviour in closed analytical form. The ratio ψ_n/B_n of the isotropic fluidity obtained with the VPSC model (on an isotropic fabric) to the grain reference fluidity ψ_n must be computed. In the linear case, Meyssonnier and Philip [67] derived the following relation when $\gamma = 1$:

$$\frac{\psi_1}{B_1} = \frac{1 + \sqrt{1 + 24\beta}}{6\beta}. \tag{32}$$

This relation can be used to choose appropriate values of grain parameter β when $\gamma = 1$. As an example, the expected experimental value of 10 is obtained for $\beta = 0.04$ and $\gamma = 1$ [67]. In the non-linear case with the tangent linearisation scheme of the VPSC, Castelnau and others [9] estimated from a comparison with experimental tests that the RRSS for the pyramidal and prismatic planes should be 70 times larger than the basal plane RRSS ($\tau_0^{pr} \approx \tau_0^{py} \approx 70\tau_0^b$).

5.1.3 Topological models

For this particular class of homogenization models, the fabric description contains some topological information so that the neighbourhood is taken into account to estimate the stress and strain-rate of a particular grain. Azuma and Goto-Azuma [5] and Thorsteinsson [87] have developed topological models in which the fabric description is discrete and the grain deforms only by basal glide with $n = 3$. In both approaches, the local deviatoric stress is evaluated from the macroscopic one as:

$$S_{ij} = \alpha_{ij}\bar{S}_{ij} \quad \text{(no sum)}, \tag{33}$$

where α_{ij} is the neighbourhood interaction coefficient tensor.

In Azuma and Goto-Azuma [5], the neighbourhood interaction coefficients are estimated as

$$\alpha_{ij} = \frac{\ll r_{ij}^s \gg}{r_{ij}^s}, \tag{34}$$

where $\ll . \gg$ denotes the local average over the neighbour grains only, and $\boldsymbol{r}^s$ is the Schmid tensor (3) for one particular direction in the basal plane, determined as the maximum resolved shear-stress direction when the macroscopic stresses act on the grain.

Thorsteinsson [87] has adopted a scalar neighbourhood interaction coefficient, defined as:

$$\alpha_{ij} = \alpha = \left(\zeta + \xi \frac{\ll |\sum_s (\boldsymbol{r}^s : \bar{\boldsymbol{S}})\boldsymbol{b}^s| \gg}{|\sum_s (\boldsymbol{r}^s : \bar{\boldsymbol{S}})\boldsymbol{b}^s|}\right) \frac{1}{(\zeta + 6\xi)}, \tag{35}$$

where $\ll . \gg$ denotes the local average over the six neighbours, and $\sum_s$ is the sum over the three slip systems of the basal plane. The two parameters ζ and ξ allow to modify the relative influence of the 6 neighbours: $(\zeta, \xi) = (1, 0)$ reduces to the uniform stress model, when $(\zeta, \xi) = (6, 1)$ the centre crystal contributes as much as all the 6 neighbours and when $(\zeta, \xi) = (1, 1)$ the centre crystal contributes as much as each of the neighbours. Note that the fabric evolution, as well as grain growth, rotation and dynamic recrystallization are implemented in Thorsteinsson's model [87].

Azuma and Goto-Azuma [5] have first highlighted the possible directional effects of anisotropy on the formation of stratigraphic disturbances. By using their polycrystalline law, they have shown that at a deeper part of an ice-sheet, where a single-maximum fabric develops, a positive vertical strain-rate can be produced with only a horizontal shear stress as far as the bedrock is not flat. Using the feature that a polycrystal with a single maximum fabric is easier to shear but harder to compress, they noticed that a small misorientation of the mean orientation of the c-axes could induce disturbances of the layers. For a vertical variation of the mean orientation, both layer thinning and thickening can occur depending on the mean orientation of the c-axis. If it varies horizontally, then layer folding or boudinage could occur. These two scenarios are only qualitative because in [5] the complex interaction from the surrounding layers was completely neglected.

The so-called cellular automaton models [30, 55] can also be included in the class of the topological models. Based on a cellular automaton algorithm, this approach allows the modelling of several competing processes acting on the fabric evolution, like deformation,

grain growth and continuous and discontinuous recrystallizations. For numerical reasons, applications are limited to two-dimensional thin section, and the stress is assumed uniform in all the grains, which is the main difference to the full-field models presented below.

5.2 Phenomenological models

In a phenomenological model, an anisotropic macroscopic formulation for the polycrystal law is postulated. To be usable, the rheological parameters that enter this law have to be evaluated as a function of the fabric. The form of the law is assumed to be restricted to particular kinds of anisotropic symmetries (orthotropy, transverse isotropy or even isotropy), and the approaches mainly differ on the way the rheological parameters and the fabric are linked. In the Morland and Staroszczyk approach [69, 70, 71, 72, 80, 81, 83, 84], the anisotropic parameters are solely phenomenological functions of the deformation, and there is no direct link with a fabric descriptor. The limit values of the strain functions are evaluated from experimental results or by comparison with an homogenization model [82].

On the contrary, the six rheological parameters entering the Gillet-Chaulet and others [40] law are simply fitted using a homogenization model, like the VPSC model presented above. In the first formulation, the fabric was described using the parameters of the PODF (24) [40], but this approach was found not to be efficient for the fabric evolution, so that the fabric was later described by the use of the second orientation tensor [41].

In the approach of Placidi and Hutter [79], the Glen's flow law collinearity between strain-rate and stress tensors is assumed to be conserved, and the anisotropy is taken into account by introducing an anisotropic enhancement factor. This anisotropic enhancement factor is a function of the so-called *deformability* of the polycrystal, evaluated from the fabric and the actual macroscopic stress. The anisotropic enhancement factor varies from 0 for a single maximum fabric under compression up to a maximum value E_s for the same fabric but solicited by simple shear.

The main interest of these models is their numerical efficiency, which allow their implementation in flow models as presented in Section 6.

5.3 Full-field models

The full-field models solve properly the Stokes equations using either classical Finite Element methods [65, 68] or Fast-Fourier Transforms [56, 57]. The latter has better performance than a Finite Element calculation for the same purpose and resolution, but only works for periodic boundary conditions. In such an approach, each crystal is decomposed in many elements, allowing to infer the stress and strain-rate heterogeneity at the microscopic scale. As an important result, these models show that, for a given orientation, the mean strain-rate and stress are strongly dependent on the neighbour grain orientations. All the same, the average value of all grains having the same orientation is still dependent on this orientation. In other words, certainly because the ice is strongly anisotropic, the neighbourhood influence does not counteract the orientation influence when looking to average behaviour of a large number of grains having the same orientation, but only induce a strong variability.

The FFT results in [57] clearly contradict the statement made by Faria and co-authors [28, 29, 31] that stress and strain-rate of a species, *i.e.* an ensemble of grains having the same orientation, should be independent of its orientation because of the huge number of grains belonging in the same species. As discussed by Gagliardini [33], the assumption made by Faria and others seems to be not insignificant and should be comparable to a uniform strain-rate or Taylor assumption in the framework of the homogenization model (for a complete discussion of this subject, see also the reply to Gagliardini's comment [33] by Faria and others [32]).

5.4 Fabric evolution

When the fabric is described using the discrete approach, the strain-rate and the spin for each constituent can be evaluated from the homogenization model and the grain $\boldsymbol{c}-$axis rotation is simply calculated from Equation (7) [13, 87, 91]. This formula also holds for evaluating the $\boldsymbol{c}-$axis evolution for the full-field models [65].

Using an ODF, Gödert and Hutter [45] have proposed to adopt the following equation for the local balance of the ODF:

$$\dot{f} + \mathrm{div}_{\boldsymbol{c}}(\dot{\boldsymbol{c}} f) = \pi^f + \mathrm{div}_{\boldsymbol{x}}\, \Psi_x^f + \mathrm{div}_{\boldsymbol{c}}\, \Psi_c^f\,, \qquad (36)$$

where $\mathrm{div}_{\boldsymbol{c}}$ and $\mathrm{div}_{\boldsymbol{x}}$ denote the divergence operator in the orientation and Cartesian spaces, respectively, π^f is a production of orientation, Ψ_c^f is associated with the diffusion of orientation in the orientation space and Ψ_x^f describes diffusion of crystals from one region to the neighbouring one. Such production and diffusion terms should be used to take into account the different recrystallization processes. Nevertheless, the continuity equation (12) only holds when these terms are neglected.

The PODF (23), (24) and (25) have been used to express the fabric evolution equation as a set of PODF parameter evolution equations for some special flow conditions and under the static assumption. This is achieved by replacing f in Equation (36) by the PODF expression. Then, a set of equations for the evolution of the parameters is derived by choosing as many particular orientations as the number of parameters in the PODF. Therefore, the resulting parameter evolution equations are not necessarily unique. Gagliardini and Meyssonnier [38] have shown that, in the case of 2D plane-strain flow, this method leads to a unique set of three equations for the three parameters k_1, k_2 and φ_0 for the PODF (24). This result was not achieved in a more general 3D flow. Thorsteinsson and others [89] have derived a simple

equation for the cone angle α in (25), by a straight-line fit of the results obtained with a discrete model [87].

Using the orientation tensor, the fabric evolution can be described at the macroscopic scale from the temporal derivation of the second order orientation tensor (14), as:

$$\dot{\boldsymbol{a}}^{(2)} = < \boldsymbol{c} \otimes \dot{\boldsymbol{c}} > + < \dot{\boldsymbol{c}} \otimes \boldsymbol{c} > \ . \tag{37}$$

The rotation rate $\dot{\boldsymbol{c}}$ of the $\boldsymbol{c}-$axis given by (7), is a function of the microscopic spin and strain-rate and should therefore be expressed as a function of macroscopic quantities if one wants to derive an explicit equation for the evolution of the second order orientation tensor. This is simply achieved for the Taylor model and also for the static one for which $\boldsymbol{D} = \psi_n / 2\tau^{n-1} \bar{\boldsymbol{S}}$. For intermediate models, Gödert [44], and Gillet-Chaulet and others [41], have proposed to adopt the following expression for the rotation rate of the orientation of a crystal:

$$\dot{\boldsymbol{c}} = \bar{\boldsymbol{W}} \cdot \boldsymbol{c} - [\bar{\boldsymbol{C}} \cdot \boldsymbol{c} - (\boldsymbol{c}^T \cdot \bar{\boldsymbol{C}} \cdot \boldsymbol{c}) \boldsymbol{c}] \, , \tag{38}$$

where $\bar{\boldsymbol{C}} = (1-\alpha) \bar{\boldsymbol{D}} + \alpha \psi_n \tau^{n-1} \bar{\boldsymbol{S}} / 2$ is a tensor, equivalent to a strain-rate, intermediate between the Taylor and static strain-rates. The scalar *interaction parameter* α allows to describe intermediate fabric evolution, from the Taylor case ($\alpha = 0$) to the static case ($\alpha = 1$). In [44], the macroscopic stress and strain-rate are evaluated using the static model, whereas Gillet-Chaulet and others [41] used the VPSC approximation.

Using this intermediate notation for the rotation rate of the orientation of a crystal, its follows from (37) that the evolution of the second order orientation tensor reads:

$$\begin{aligned} \dot{\boldsymbol{a}}^{(2)} = & \bar{\boldsymbol{W}} \cdot \boldsymbol{a}^{(2)} - \boldsymbol{a}^{(2)} \cdot \bar{\boldsymbol{W}} - (\bar{\boldsymbol{C}} \cdot \boldsymbol{a}^{(2)} - \boldsymbol{a}^{(2)} \cdot \bar{\boldsymbol{C}}) \\ & + 2 \boldsymbol{a}^{(4)} : \bar{\boldsymbol{C}} \, . \end{aligned} \tag{39}$$

Equation (39) for the evolution of $\boldsymbol{a}^{(2)}$ involves the fourth-order orientation tensor $\boldsymbol{a}^{(4)}$. The same procedure applied to $\boldsymbol{a}^{(4)}$ would show that $\dot{\boldsymbol{a}}^{(4)}$ depends on $\boldsymbol{a}^{(6)}$, and, in general, that any evolution equation for an even-order orientation tensor $\dot{\boldsymbol{a}}^{(2p)}$ will involve the next higher even-order orientation tensor $\boldsymbol{a}^{(2p+2)}$. To obtain a closed set of equations we must stop at a given order $2p$ and make a so-called *closure approximation*, *i.e.* postulate a relation between $\boldsymbol{a}^{(2p+2)}$ and $\boldsymbol{a}^{(2p)}$. Using a closure approximation for $\boldsymbol{a}^{(4)}$ leads to the assumption of macroscopic orthotropy [15].

Orientation tensors are widely used to provide a compact representation of fiber orientations in reinforced composites, and many closure approximations have been proposed (see for example [1, 14, 15] and references therein). A simple form for the closure approximation, known as the *quadratic closure*, is:

$$\tilde{\boldsymbol{a}}^{(4)} = \boldsymbol{a}^{(2)} \otimes \boldsymbol{a}^{(2)} \, . \tag{40}$$

Note that the quadratic closure does not respect the symmetries of $\boldsymbol{a}^{(4)}$ and is only exact for a perfect single maximum fabric.

A second approach, the *linear closure*, is built from all the possible products of $\boldsymbol{a}^{(2)}$ and the identity tensor $\boldsymbol{I}$ that respect the symmetries of $\boldsymbol{a}^{(4)}$:

$$\begin{aligned} 7 \hat{a}^{(4)}_{ijkl} = & -\frac{1}{5} (\delta_{ij}\delta_{kl} + \delta_{ik}\delta_{jl} + \delta_{il}\delta_{jk}) + a^{(2)}_{ij} \delta_{kl} \\ & + a^{(2)}_{ik} \delta_{jl} + a^{(2)}_{il} \delta_{jk} + a^{(2)}_{kl} \delta_{ij} + a^{(2)}_{jl} \delta_{ik} + a^{(2)}_{jk} \delta_{il} \, . \end{aligned} \tag{41}$$

Advani and Tucker [1] have proposed an *hybrid closure* constructed from the two previous ones:

$$\boldsymbol{a}^{(4)} = (1 - \alpha_f) \hat{\boldsymbol{a}}^{(4)} + \alpha_f \tilde{\boldsymbol{a}}^{(4)} \, , \tag{42}$$

where $2\alpha_f = 3\boldsymbol{a}^{(2)} : \boldsymbol{a}^{(2)} - 1$. Since $\alpha_f = 1$ for a single maximum fabric and $\alpha_f = 0$ for an isotropic one, the hybrid closure is exact for both cases. The hybrid closure was applied to ice by Gödert [44].

Gillet-Chaulet and others [41] have used the *Invariant-Based Optimal Fitting* (IBOF) closure from Chung and Kwon [14]. Its general form is

$$\begin{aligned} \boldsymbol{a}^{(4)} = & \beta_1 (\boldsymbol{I} \otimes \boldsymbol{I})^D + \beta_2 (\boldsymbol{I} \otimes \boldsymbol{a}^{(2)})^D \\ & + \beta_3 (\boldsymbol{a}^{(2)} \otimes \boldsymbol{a}^{(2)})^D + \beta_4 (\boldsymbol{I} \otimes \boldsymbol{a}^{(2)} \cdot \boldsymbol{a}^{(2)})^D \\ & + \beta_5 (\boldsymbol{a}^{(2)} \otimes \boldsymbol{a}^{(2)} \cdot \boldsymbol{a}^{(2)})^D \\ & + \beta_6 (\boldsymbol{a}^{(2)} \cdot \boldsymbol{a}^{(2)} \otimes \boldsymbol{a}^{(2)} \cdot \boldsymbol{a}^{(2)})^D \, , \end{aligned} \tag{43}$$

where $\boldsymbol{I}$ is the identity tensor, and the six functions β_i are functions of the second and third invariants of $\boldsymbol{a}^{(2)}$, denoted by II and III respectively. It can be shown that, owing to the symmetries of $\boldsymbol{a}^{(4)}$ and the normalisation condition $\mathrm{tr}\, \boldsymbol{a}^{(2)} = 1$, only 3 functions β_i are independent. Following Chung and Kwon [14], Gillet-Chaulet and others [41] have taken the three independent functions as complete polynomials of degree 5 in II and III, so that 63 parameters need to be determined. By adding two other relations to insure that the IBOF closure approximation is exact for perfectly aligned fabrics and girdle fabrics, this number is reduced to 61.

Gillet-Chaulet and others [41] have computed these 61 coefficients so that $\boldsymbol{a}^{(4)}$ given by (43) fits the fourth order orientation tensor calculated by using PODF (24) (see Annex C of [39] for the values of the 61 coefficients). The IBOF closure is much more accurate than the hybrid closure and, in the linear case ($n = 1$), it conducts to the same fabric evolution than the one obtained by solving the evolution equations for the parameters of the PODF (24), but in a much faster way.

Both the hybrid and IBOF closures assume implicitly that the fabric is orthotropic. To avoid this hypothesis, which should not be so strong for polycrystal ice, one can compute the evolution of $\boldsymbol{a}^{(4)}$, but must then adopt a closure approximation between $\boldsymbol{a}^{(4)}$ and $\boldsymbol{a}^{(6)}$ [50].

6 Flow models of anisotropic polar ice

In order to study the influence of ice anisotropy on the flow of ice-sheets, a modelling efforts have been made in

order to implement anisotropic laws in flow models, and for a few applications, the anisotropic flow laws have also been coupled with the strain-induced fabric evolution.

6.1 Flow of anisotropic ice

In the framework of the Shallow Ice Approximation (SIA) [49], initially developed for isotropic ice, Mangeney and Califano [62] have proposed the extension to anisotropic ice of the SIA up to the second order. They have adopted the static transversely isotropic law of Lliboutry [60], in which the fabric is described by the PODF (21). The symmetry axis of the fabric coincides with the vertical axis, and only vertical changes of the fabric strength are allowed. Mangeney and Califano [62] have shown that the zero-order approximation of the anisotropic SIA is fully equivalent to the isotropic SIA with an enhancement factor. However, when the second-order correction is calculated, the isotropic SIA with an enhancement factor does not correspond to the anisotropic SIA anymore. By comparing the anisotropic SIA to an *exact* solution, Mangeney and Califano [62] have shown that for a perturbed bedrock, the second-order approximation is needed.

These developments were further extended by Philip and Meyssonnier [77] to the case of a non-vertical symmetry axis of the fabric. They have shown that the diagonal components of the deviatoric stress can be of the same order as the shear stress when the material symmetry axis is not vertical, clearly indicating that the above conclusion by Mangeney and Califano regarding the enhancement factor is only valid in the restricted case of a vertical material symmetry axis. Moreover, Philip and Meyssonnier have shown that the solutions at orders greater than zero remain negligible in the particular case of a linear rheology and a flat bed.

Using the same Lliboutry's polycrystal model as in [62], Mangeney and others [63, 64] have developed a two-dimensional isothermal full-Stokes model restricted to Newtonian behaviour, without [63] and with [64] taking into account the free surface evolution as a function of an imposed accumulation. In this approach, the fabric is given and is assumed to be a function of the relative depth only. In [64], they have shown that the effect of anisotropy is partly smoothed out by the change of the free surface which is flatter in the anisotropic case than in the isotropic case. In the particular case of a sinusoidal bedrock, the anisotropic ice above the bump is found to be younger by more than 10 % compared to the isotropic ice, and in the holes of the relief it is older by more than 100 %.

More recently, Pettit and others [76] have developed a flow model, in which the ice fabric is described using the cone-angle PODF (25), and the anisotropic ice behaviour is inferred from analytical solutions derived under the static assumption for simple loading cases in [86]. Because Pettit and others [76] consider complex load conditions in their flow model, these analytical results were linearised, and the flow non-linearity was re-introduced by the use of an isotropic bulk effective viscosity derived from Glen's law. Assuming that the cone-angle profile is only a function of reduced depth, this non-linear model was applied to study the flow near an ice divide. They have shown that a strong crystal fabric always increases the amplitude of the existing arch in the isochrones, the so-called Raymond bump, relative to the isotropic case. They have confirmed that with a linear flow law, no arch exists in either the anisotropic or isotropic case.

6.2 Flow and fabric evolution of anisotropic ice

Gödert [43] and Gödert and Hutter [46] have developed an anisotropic flow model with induced anisotropy using a coupled Finite-Element Finite-Volume approach. In their approach, the Newtonian orthotropic behaviour of ice is inferred from the static model, the fabric is described using the PODF (23) and its evolution is intermediate between the Taylor and static models (Equation (38)). As a first application, this flow model was applied to a rectangular domain 10 times wider than thick in order to reproduce the stationary plane flow in the vicinity of an ice divide. The results obtained at the divide were shown to reproduce well the evolution of fabric along the GRIP core.

Also using a static Newtonian orthotropic model and a fabric given by the PODF (24), Gagliardini and Meyssonnier have applied their anisotropic flow model to a 2D synthetic ice-sheet geometry [36] and to study the fabric evolution along the GRIP ice core [37]. In this later application, they have shown, by comparing the fabric evolution obtained with the 2D flow model to the fabric evolution inferred from a Dansgaard-Johnsen one dimensional flow model [16], that the flow conditions clearly influence the fabric evolution. Because of this complex coupling between the flow and the fabric, the use of a trivial evaluation of the strain-rate history, like a one dimensional Dansgaard-Johnsen model, renders the application of any polycrystalline model open to criticism when comparing measured and modeled fabrics.

Gillet and others [41] have presented a 2D isothermal orthotropic flow model with induced anisotropy and free surface evolution. The polycrystal behaviour is inferred from an orthotropic Newtonian phenomenological model using the VPSC solution to fit the viscosity parameters. The fabric is described by the use of the orientation tensors. The velocity, pressure and fabric fields, as well as the free surface elevation, were calculated in a coupled way for a synthetic ice-sheet geometry, consisting of sinusoidal bedrock elevation. Their results show that, due to the bedrock irregularities, the ice fabric field presents a strong spatial variability. The same model was later applied to quantify the influence of a difference in the initial surface viscosity on the fabric development [21].

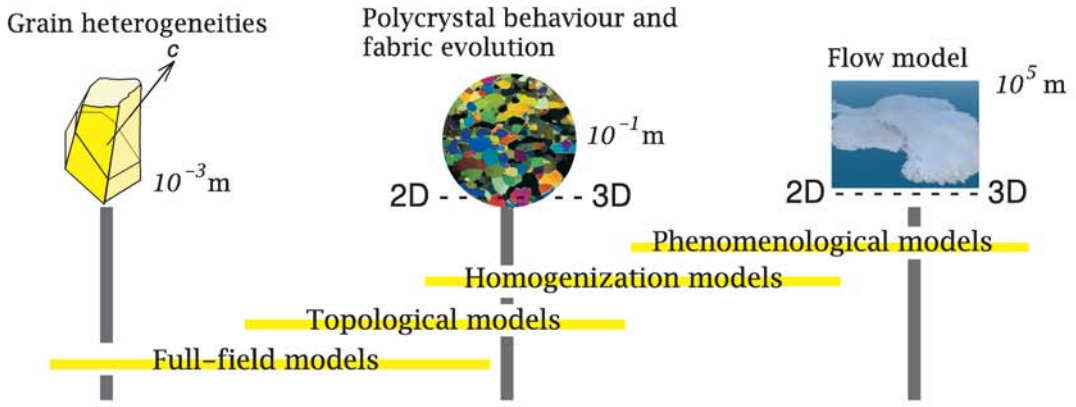

Figure 4: *Typical size of the modelled object and schematic classification of the adapted applications for each polycrystal model.*

The test consisted in prescribing a time-dependent initial surface viscosity, supposed to mimic the effect of impurities and/or grain size which vary from glacial to inter-glacial periods. As expected, as far as some shear deformation is possible, a positive feedback is observed, *i.e.* an initially softer layer experiences more shear, so that its fabric is more concentrated and therefore easier to shear, and so on. The model qualitatively reproduces the observed strengthening of the fabric during Termination II around 1750 m at Dome C, indicating that the Dome C ice certainly underwent shear deformation.

Morland and Staroszczyk [73] have implemented their phenomenological law in a steady radial ice-sheet flow model. The velocities, the fabric evolution and the free surface elevation are calculated in a coupled way, assuming a given temperature profile. In their approach, the fabric evolution is simulated by the evolution of the left Cauchy-Green strain tensor, leading to three independent evolution equations. For the flow solution, the typical magnitudes of physical variables are studied, and the resulting equations are simplified by neglecting the terms lower than the maximum bedrock slope. The flow of anisotropic and isotropic ice is compared in the particular case of a steady radial geometry, for a flat bed, a bed with a single symmetric hump and a bed with a single symmetric basin.

7 Conclusion

A review of a large number of models has been presented, from crystal models up to anisotropic flow models. It appears that in glaciology, most of the modelling consists in the development of homogenization models under different assumptions, using different crystal models.

Regarding the polycrystal models, Figure 4 is a tentative classification of the different polycrystal models as a function of their application. This classification comes from both the numerical cost and the quality of the solution at the different scales for each of the presented polycrystal models.

In the near future, investigation of the interaction between all these different models should be a good strategy. For example, results from full-field models can be used to validate an homogenization model, which itself can serve as an input to the development of a phenomenological model. In the reverse, streamlines and associated strain histories inferred from an anisotropic flow model can serve as input to an homogenization model for the computation of the fabric evolution in an ice core.

Acknowledgements

This work is a contribution to the 'European Project for Ice Coring in Antarctica' (EPICA), a joint ESF (European Science Foundation) / EC scientific programme, funded by the European Commission under the Environment and Climate Program contract ENV4-CT95-0074 and by national contributions from Belgium, Denmark, France, Germany, Italy, the Netherlands, Norway, Sweden, Switzerland and the United Kingdom. The authors wish to thank the anonymous referee, the editor T. Hondoh and R. Greve for the English corrections.

References

[1] S. G. Advani and C. L. Tucker III. The use of tensors to describe and predict fiber orientation in short fiber composites. *J. Rheol.*, 31(8):751–784, 1987.

[2] R. B. Alley. Fabrics in polar ice sheets-Development and prediction. *Science*, 240:493–495, 1988.

[3] R. B. Alley. Flow-law hypotheses for ice-sheet modeling. *J. Glaciol.*, 38(129):245–256, 1992.

[4] R. B. Alley, A. J. Gow, and D. A. Meese. Mapping c-axis fabrics to study physical processes in ice. *J. Glaciol.*, 41(137):1995, 1995.

[5] N. Azuma and K. Goto-Azuma. An anisotropic flow law for ice-sheet ice and its implications. *Ann. Glaciol.*, 23:202–208, 1996.

[6] N. Azuma and A. Higashi. Formation processes of ice fabric pattern in ice sheets. *Ann. Glaciol.*, 6:130–134, 1985.

[7] N. Azuma, Y. Wang, K. Mori, H. Narita, T. Hondoh, H. Shoji, and O. Watanabe. Textures and fabrics in the Dome F (Antarctica) ice core. *Ann. Glaciol.*, 29:163–168, 1999.

[8] N. Azuma, Y. Wang, Y. Yoshida, H. Narita, T. Hondoh, H. Shoji, and O. Watanabe. Crystallographic analysis of the Dome Fudji ice core. In T. Hondoh, editor, *Physics of Ice Core Records*, pages 45–61. Hokkaido University Press, Sapporo, 2000.

[9] O. Castelnau, G. R. Canova, R. A. Lebensohn, and P. Duval. Modelling viscoplastic behavior of anisotropic polycrystalline ice with a self-consistent approach. *Acta. Mater.*, 45(11):4823–4834, 1997.

[10] O. Castelnau and P. Duval. Simulations of anisotropy and fabric development in polar ices. *Ann. Glaciol.*, 20:277–282, 1994.

[11] O. Castelnau, P. Duval, R. A. Lebensohn, and G. Canova. Viscoplastic modeling of texture development in polycrystalline ice with a self-consistent approach : Comparison with bound estimates. *J. Geophys. Res.*, 101(6):13,851–13,868, 1996.

[12] O. Castelnau, H. Shoji, A. Mangeney, H. Milsch, P. Duval, A. Miyamoto, K. Kawada, and O. Watanabe. Anisotropic behavior of GRIP ices and flow in central Greenland. *Earth Planet. Sci. Lett.*, 154(1-4):307–322, 1998.

[13] O. Castelnau, Th. Thorsteinsson, J. Kipfstuhl, P. Duval, and G. R. Canova. Modelling fabric development along the GRIP ice core, central Greenland. *Ann. Glaciol.*, 23:194–201, 1996.

[14] D. H. Chung and T. H. Kwon. Invariant-based optimal fitting closure approximation for the numerical prediction of flow-induced fiber orientation. *J. Rheol.*, 46(1):169–194, 2002.

[15] J. S. Cintra and C. L. Tucker III. Orthotropic closure approximations for flow-induced fiber orientation. *J. Rheol.*, 39(10):1095–1122, 1995.

[16] W. Dansgaard and S. J. Johnsen. A flow model and a time scale for the ice core from Camp Century, Greenland. *J. Glaciol.*, 8(53):215–223, 1969.

[17] S. de La Chapelle, O. Castelnau, V. Ya. Lipenkov, and P. Duval. Dynamic recrystallization and texture development in ice as revealed by the study of deep ice cores in Antarctica and Greenland. *J. Geophys. Res.*, 103(B3):5091–5105, 1998.

[18] S. M. Dinh and R. C. Armstrong. A rheological equation of state for semiconcentrated fiber suspensions. *J. Rheol.*, 28(3):207–227, 1984.

[19] C. S. M. Doake and E. W. Wolff. Flow law in polar ice sheets. *Nature*, 314:255–257, 1985.

[20] G. Durand, O. Gagliardini, T. Thorsteinsson, A. Svensson, J. Kipfstuhl, and D. Dahl-Jensen. Ice microstructure and fabric: an up to date approach to measure textures. *J. Glaciol.*, 52(179):619–630, 2006.

[21] G. Durand, F. Gillet-Chaulet, A. Svensson, O. Gagliardini, S. Kipfstuhl, J. Meyssonnier, F. Parrenin, P. Duval, and D. Dahl-Jensen. Change in ice rheology during climate variations – implications for ice flow modelling and dating of the EPICA Dome C core. *Clim. Past*, 3(1):155–167, 2007.

[22] G. Durand, F. Graner, and J. Weiss. Deformation of grain boundaries in polar ice. *Eur. Phys. Lett.*, 67(6):1038–1044, 2004.

[23] G. Durand, A. Svensson, S. Kipfstuhl, A. Persson, O. Gagliardini, F. Gillet-Chaulet, J. Sjolte, M. Montagnat, and D. Dahl-Jensen. Evolution of the texture along the EPICA Dome C ice core. *This issue.*

[24] G. Durand, J. Weiss, V. Lipenkov, JM Barnola, G. Krinner, F. Parrenin, B. Delmonte, C. Ritz, P. Duval, R. Röthlisberger, and M. Bigler. Effect of impurities on grain growth in cold ice sheets. *J. Geophys. Res.*, 111:F01015, 2006.

[25] P. Duval. Creep and fabrics of polycrystalline ice under shear and compression. *J. Glaciol.*, 27(95):129–140, 1981.

[26] P. Duval, M. F. Ashby, and I. Anderman. Rate-controlling processes in the creep of polycrystalline ice. *J. Phys. Chem.*, 87(21):4066–4074, 1983.

[27] P. Duval and O. Castelnau. Dynamic recrystallization of ice in polar ice sheets. *J. Physique IV (suppl. J. Phys. III), C3*, 5:197–205, 1995.

[28] S. H. Faria. Creep and recrystallization of large polycrystalline masses. I. General continuum theory. *Proc. R. Soc. A*, 462:1493–1514, 2006.

[29] S. H. Faria. Creep and recrystallization of large polycrystalline masses. III: Continuum theory of ice sheets. *Proc. R. Soc. A*, 462:2797–2816, 2006.

[30] S.H. Faria, D. Ktitarev, and K. Hutter. Modelling evolution of anisotropy in fabric and texture of polar ice. *Ann. Glaciol.*, 35:545–551, 2002.

[31] S. H. Faria, G. M. Kremer, and K. Hutter. Creep and recrystallization of large polycrystalline masses. II. Constitutive theory for crystalline media with transversely isotropic grains. *Proc. R. Soc. A*, 462:1699–1720, 2006.

[32] S. H. Faria, G. M. Kremer, and K. Hutter. Reply to Gagliardini's comment on 'Creep and recrystallization of large polycrystalline masses' by Faria and co-authors. *Proc. R. Soc. A*, 464:2803–2809, 2008.

[33] O. Gagliardini. Comments on the papers 'Creep and recrystallization of large polycrystalline masses' from Faria and co-authors (2006). *Proc. R. Soc. A*, 464:289–291, 2008.

[34] O. Gagliardini, G. Durand, and Y. Wang. Grain area as a statistical weight for polycrystal constituents. *J. Glaciol.*, 50(168):87–95, 2004.

[35] O. Gagliardini and J. Meyssonnier. Analytical derivations for the behaviour and fabric evolution of a linear orthotropic ice polycrystal. *J. Geophys. Res.*, 104(B8):17,797–17,809, 1999.

[36] O. Gagliardini and J. Meyssonnier. Plane flow of an ice sheet exhibiting strain-induced anisotropy. *Hutter K., Y. Wang, H. Beer (eds.), Advances in Cold-Region Thermal Engineering and Sciences: Technological, Environmental and Climatological Impact. Berlin, etc., Springer-Verlag (Lecture Notes in Physics* **533***)*, pages 171–182, 1999.

[37] O. Gagliardini and J. Meyssonnier. Simulation of anisotropic ice flow and fabric evolution along the GRIP-GISP2 flow line (central greenland). *Ann. Glaciol.*, 30:217–223, 2000.

[38] O. Gagliardini and J. Meyssonnier. Lateral boundary conditions for a local anisotropic ice flow model. *Ann. Glaciol.*, 35:503–509, 2002.

[39] F. Gillet-Chaulet. *Modélisation de l'écoulement de la glace polaire anisotrope et premières applications au forage de Dôme C*. PhD thesis, Thèse de Doctorat de l'Université Joseph Fourier-Grenoble I, 2006.

[40] F. Gillet-Chaulet, O. Gagliardini, J. Meyssonnier, M. Montagnat, and O. Castelnau. A user-friendly anisotropic flow law for ice-sheet modelling. *J. Glaciol.*, 41(172):3–14, 2005.

[41] F. Gillet-Chaulet, O. Gagliardini, J. Meyssonnier, T. Zwinger, and J. Ruokolainen. Flow-induced anisotropy in polar ice and related ice-sheet flow modelling. *J. Non-Newtonian Fluid Mech.*, 134:33–43, 2006.

[42] P. Gilormini, M. V. Nebozhyn, and P. Ponte Castañeda. Accurate estimates for the creep behavior of hexagonal polycrystals. *Acta Mater.*, 49:329–337, 2001.

[43] G. Gödert. A meso-macro model for the description of induced anisotropy of natural ice, including grain interaction. *Advances in Cold-Region Thermal Engineering and Sciences*, pages 183–196, 1999.

[44] G. Gödert. A mesoscopic approach for modelling texture evolution of polar ice including recrystallization phenomena. *Ann. Glaciol.*, 37:23–28, 2003.

[45] G. Gödert and K. Hutter. Induced anisotropy in large ice shields: Theory and its homogenization. *Cont. Mech. Thermodyn.*, 10:293–318, 1998.

[46] G. Gödert and K. Hutter. Material update procedure for planar transient flow of ice with evolving anisotropy. *Ann. Glaciol.*, 30:107–114, 2000.

[47] A. J. Gow and T. C. Williamson. Rheological implications of the internal structure and crystal fabrics of the West Antarctic ice sheet as revealed by deep core drilling at Byrd station. *Geol. Soc. Am. Bull.*, 87(12):1665–1677, 1976.

[48] F. J. Humphreys and M. Haterly. *Recrystallization and Related Annealing Phenomena*. Pergamon Tarrytown, N. Y., 1995.

[49] K. Hutter. *Theoretical Glaciology: Material Science of Ice and the Mechanics of Glaciers and Ice Sheets*. D. Reidel Publishing Company, Terra Scientific Publishing Company (ISBN 90 277 1473 8), 1983.

[50] D. A. Jack and D. E. Smith. An invariant based fitted closure of the sixth-order orientation tensor for modeling short-fiber suspensions. *J. Rheology*, 49:1091, 2005.

[51] T. H. Jacka. The time and strain required for development of minimum strain rates in ice. *Cold Reg. Sci. Technol.*, 3:261–268, 1984.

[52] T. H. Jacka and J. Li. Flow rates and crystal orientation fabrics in compression of polycrystalline ice at low temperatures and stresses. In T. Hondoh, editor, *Physics of Ice Core Records*, pages 83–102. Hokkaido University Press, Sapporo, 2000.

[53] W. B. Kamb. The glide direction in ice. *J. Glaciol.*, 3(30):1097–1106, 1961.

[54] U. F. Kocks, C. N. Tomé, and H.-R. Wenk. *Texture and Anisotropy. Preferred Orientations in Polycrystals and Their Effect on Materials Properties*. Cambridge University Press (ISBN 0 521 46516 8), 1998.

[55] D. Ktitarev, G. Gödert, and K. Hutter. Cellular automaton model for recrystallization, fabric, and texture development in polar ice. *J. Geophys. Res.*, 107(B8), 2002.

[56] R. Lebensohn, Y. Liu, and P. Ponte Castañeda. On the accuracy of the self-consistent approximation for polycrystals: comparison with full-field numerical simulations. *Acta Materialia*, 52(18):5347–5361, 2004.

[57] R. A. Lebensohn, Y. Liu, and P. P. Castañeda. Macroscopic properties and field fluctuations in model power-law polycrystals: full-field solutions versus self-consistent estimates. *Proc. R. Soc. Lond. A*, 460:1381–1405, 2004.

[58] V. Ya. Lipenkov, N. I. Barkov, P. Duval, and P. Pimienta. Crystalline texture of the 2083m ice core at Vostock Station, Antarctica. *J. Glaciol.*, 35(121):392–398, 1989.

[59] V. Ya. Lipenkov, A. N. Salamatin, and P. Duval. Bubbly-ice densification in ice sheets: II. Applications. *J. Glaciol.*, 43(145):397–407, 1997.

[60] L. Lliboutry. Anisotropic, transversely isotropic non linear viscosity of rock ice and rheological parameters inferred by homogenization. *Int. J. Plast.*, 9:619–632, 1993.

[61] L. Lliboutry and P. Duval. Various isotropic and anisotropic ices found in glacier and polar ice caps and their corresponding rheologies. *Annales Geophysicae*, 3(2):207–224, 1985.

[62] A. Mangeney and F. Califano. The shallow ice approximation for anisotropic ice: formulation and limits. *J. Geophys. Res.*, 103(B1):691–705, 1998.

[63] A. Mangeney, F. Califano, and O. Castelnau. Isothermal flow of an anisotropic ice sheet in the vicinity of an ice divide. *J. Geophys. Res.*, 101(12):28,189–28,204, 1996.

[64] A. Mangeney, F. Califano, and K. Hutter. A numerical study of anisotropic, low Reynolds number, free surface flow of ice sheet modeling. *J. Geophys. Res.*, 102(B10):22,749–22,764, 1997.

[65] P. Mansuy, J. Meyssonnier, and A. Philip. Localization of deformation in polycrystalline ice: experiments and numerical simulations with a simple grain model. *Computational Materials Science*, 25(1-2):142–150, 2002.

[66] J. Meyssonnier, P. Duval, O. Gagliardini, and A. Philip. Constitutive modelling and flow simulation of anisotropic polar ice. *Straughan B., R. Greve, H. Ehrentraut and Y. Wang (Eds.), Continuum Mechanics and Applications in Geophysics and the Environment. Berlin, etc., Springer-Verlag*, 2001.

[67] J. Meyssonnier and A. Philip. A model for the tangent viscous behaviour of anisotropic polar ice. *Ann. Glaciol.*, 23:253–261, 1996.

[68] J. Meyssonnier and A. Philip. Comparison of finite-element and homogenization methods for modelling the viscoplastic behaviour of a S2-columnar-ice polycrystal. *Ann. Glaciol.*, 30:115–120, 2000.

[69] L. W. Morland. Influence of lattice distortion on fabric evolution in polar ice. *Cont. Mech. Thermodyn.*, 14(1):9–24, 2002.

[70] L. W. Morland and R. Staroszczyk. Viscous response of Polar ice with evolving fabric. *Cont. Mech. Thermodyn.*, 10:115–120, 1998.

[71] L. W. Morland and R. Staroszczyk. Strain-rate formulation of ice fabric evolution. *Ann. Glaciol.*, 37(1):35–39, 2003.

[72] L. W. Morland and R. Staroszczyk. Stress and strain-rate formulations for fabric evolution in polar ice. *Cont. Mech. Thermodyn.*, 15(1):55–71, 2003.

[73] L.W. Morland and R. Staroszczyk. Steady radial ice-sheet flow with fabric evolution. *J. Glaciol.*, 52(177):267–280, 2006.

[74] R. Obbard and I. Baker. The microstructure of meteoric ice from Vostok, Antarctica. *J. Glaciol.*, 53(180):41–62, 2007.

[75] R. Obbard, I. Baker, and K. Sieg. Using electron backscatter diffraction patterns to examine recrystallization in polar ice sheets. *J. Glaciol.*, 52(179):546–557, 2006.

[76] E. C. Pettit, T. Thorsteinsson, P. Jacobson, and E. D. Waddington. The role of crystal fabric in flow near an ice divide. *J. Glaciol.*, 53(181):277–288, 2007.

[77] A. Philip and J. Meyssonnier. Anisotropic isothermal ice-cap flow with the shallow ice approximation. *Hutter K., Y. Wang, H. Beer (eds.), Advances in Cold-Region Thermal Engineering and Sciences: Technological, Environmental and Climatological Impact. Berlin, etc., Springer-Verlag (Lecture Notes in Physics* **533***)*, pages 237–248, 1999.

[78] P. Pimienta, P. Duval, and V. Y. Lipenkov. Mechanical behaviour of anisotropic polar ice. *International Association of Hydrological Sciences, Publication 170 (Symposium on the Physical Basis of Ice Sheet Modelling, Vancouver)*, pages 57–66, 1987.

[79] L. Placidi and K. Hutter. An anisotropic flow law for incompressible polycrystalline materials. *Zeitschrift für Angewandte Mathematik und Physik (ZAMP)*, 57(1):160–181, 2006.

[80] R. Staroszczyk. An orthotropic constitutive model for secondary creep of ice. *Arch. Mech.*, 53(1):65–85, 2001.

[81] R. Staroszczyk. Strengthening and weakening of induced anisotropy in polar ice. *Proc. R. Soc. A*, 457(2014):2419–2440, 2001.

[82] R. Staroszczyk and O. Gagliardini. Two orthotropic models for strain-induced anisotropy of polar ice. *J. Glaciol.*, 45(151):485–494, 1999.

[83] R. Staroszczyk and L. W. Morland. Orthotropic viscous response of polar ice. *J. Engng. Math.*, 37:191–209, 2000.

[84] R. Staroszczyk and L. W. Morland. Plane ice sheet flow with evolving orthotropic fabric. *Ann. Glaciol.*, 30:93–101, 2000.

[85] B. Svendsen and K. Hutter. A continuum approach for modelling induced anisotropy in glaciers and ice sheets. *Ann. Glaciol.*, 23:262–269, 1996.

[86] T. Thorsteinsson. An analytical approach to deformation of anisotropic ice-crystal aggregates. *J. Glaciol.*, 47(158):507–516, 2001.

[87] T. Thorsteinsson. Fabric development with nearest-neighbor interaction and dynamic recrystallization. *J. Geophys. Res. (Solid Earth*, 107(B1), 2002.

[88] T. Thorsteinsson, J. Kipfstuhl, and H. Miller. Textures and fabrics in the GRIP ice core. *J. Geophys. Res.*, 102(C12):26,583–26,600, 1997.

[89] T. Thorsteinsson, E.D. Waddington, and R.C. Fletcher. Spatial and temporal scales of anisotropic effects in ice-sheet flow. *Ann. Glaciol.*, 37(1):40–48, 2003.

[90] M. Vallon, J.-R. Petit, and B. Fabre. Study of an ice core to the bedrock in the accumulation zone of an alpine glacier. *J. Glaciol.*, 17(75):13–28, 1976.

[91] C. J. Van der Veen and I. M. Whillans. Development of fabric in ice. *Cold Reg. Sci. Technol.*, 22(2):171–195, 1994.

[92] Y. Wang, S. Kipfstuhl, and N. Azuma. Ice fabrics study in the upper 1500 m of the Dome C deep ice core, East Antarctica. *Ann. Glaciol.*, 37:97–104, 2003.

[93] Y. Wang, T. Thorsteinsson, J. Kipfsuhl, H. Miller, D. Dahl-Jensen, and H. Shoji. A vertical girdle fabric in the NGRIP deep ice core, North Greenland. *Ann. Glaciol.*, 35:515–520, 2002.

[94] Q. S. Zheng and W. N. Zou. Orientation distribution functions for microstructures of heterogeneous materials (I): directional distribution functions and irreducible tensors. *Appl. Math. Mech.*, 22(8):865–884, 2001.